crystals

Article

Effects of NH_4SCN Additive in the $FAPbI_3$ Perovskite Films in a Sequential Deposition Method

Jorge Luis Miró-Zárate [1], Miltón Carlos Elías-Espinosa [1,*], Felipe Cervantes-Sodi [2] and Carolina Janani Diliegros-Godines [3,*]

[1] Instituto Tecnologico y de Estudios Superiores de Monterrey, Campus Santa Fe, School of Engineering and Science, Mexico City 01389, Mexico; jorge.miro@tec.mx
[2] Physics and Mathematics Department, Universidad Iberoamericana Ciudad de Mexico, Prolongación Paseo de la Reforma 880, Mexico City 01219, Mexico
[3] Instituto de Física, Benemérita Universidad Autónoma de Puebla, Apdo. Post. J-48, Puebla 72570, Pue, Mexico
* Correspondence: mielias@tec.mx (M.C.E.-E.); carolina.diliegros@correo.buap.mx (C.J.D.-G.); Tel.: +52-5591-778-000 (M.C.E.-E.)

Abstract: This study determined the effect of introducing the NH_4SCN additive in the precursor solution of PbI_2 of a sequential deposition method in an open atmosphere to form $FAPbI_3$ perovskite over a glass substrate. Adding NH_4SCN leads to different intermediate layers according to the concentration of the additive. From an adequate concentration, an ionic substitution between I^- and SCN^- is promoted, providing a unique path for nucleation and growth of $FAPbI_3$ due to significant changes in morphology. The intermediate layer with a proper amount of NH_4SCN enhanced the physical properties of $FAPbI_3$. It contributed to understanding the crystallinity and morphological conditions for favorable growth of $FAPbI_3$ directly over a glass substrate. A concentration of 40% gave rise to the biggest grain size, homogeneous morphology, higher absorption, and prevalence of black phase in the α/δ phase coexistence. As a result, the perovskite with the NH_4SCN additive showed a positive effect on the growth mechanisms and enhanced stability due to the mixed α/δ-phase and grain size ~1350 nm. The preceding makes $FAPbI_3$ film with a concentration of 40% a good option for application as stable perovskite in solar cells.

Keywords: perovskite; $FAPbI_3$; sequential deposition; ammonium thiocyanate; open atmosphere

Citation: Miró-Zárate, J.L.; Elías-Espinosa, M.C.; Cervantes-Sodi, F.; Diliegros-Godines, C.J. Effects of NH4SCN Additive in the $FAPbI_3$ Perovskite Films in a Sequential Deposition Method. *Crystals* **2023**, *13*, 795. https://doi.org/10.3390/cryst13050795

Academic Editor: Maria Gazda

Received: 28 March 2023
Revised: 6 May 2023
Accepted: 8 May 2023
Published: 10 May 2023

1. Introduction

The demand for renewable energy has been increasing in recent years. This comes along with the need to develop new solar cell technologies. Among the generations of solar cells, the third generation has been the most promising approach to having solar cells with high theoretical solar efficiencies and relatively low environmental impacts. Hybrid organic-inorganic perovskites (HOIPs) are strong candidates for large-scale application of next-generation photovoltaic technologies due to their potential low cost, high performance, and solution processability. In addition, their outstanding optoelectronic properties and increased power conversion efficiency (PCE) from 3.8% to 23.7% in just a few years [1,2] have facilitated their integration into several applications such as tandem solar cells, building-integrated photovoltaics, photovoltaic-driven catalysis, among others.

One of the most used crystalline HOIPs is the methylammonium lead halide ($MAPbI_3$), with a direct bandgap and excellent light absorption. However, $MAPbI_3$ undergoes a phase transition to a product of PbI_2 at low temperatures, it is not stable above 100 °C, suffers light and thermal degradation and it is not stable against moisture [3]. To improve $MAPbI_3$ stability issues, the exchange of organic/inorganic cation $CH_3NH_3^+$ to a slightly larger $CH(NH_2)_2^+$ has been introduced.

Another material of great interest is the formamididium lead halide ($FAPbI_3$). $FAPbI_3$ presents a symmetric perovskite structure with black trigonal photoactive α-$FAPbI_3$ phase, a time-enhanced operation stability, and awards higher thermal and photostability than $MAPbI_3$ [4]. However, $FAPbI_3$ crystallizes at room temperature as a yellow photoinactive hexagonal δ-$FAPbI_3$ phase that leads to unstable device operations accompanied by difficulty in achieving stable phase and quality films [5].

Several deposition methodologies are reported in the literature to improve the quality and stability of $FAPbI_3$, such as additive-assisted deposition, solvent engineering and sequential deposition [6–8]. The sequential deposition, upon all other methods, yields a means of crystallization control by involving an intermediate layer of PbI_2 from which perovskite reacts with the predeposited architecture, and can serve as nucleation center for the perovskite film growth [7]. However, despite the ease of manufacture and reduced material cost, a PbI_2 incomplete conversion to $FAPbI_3$, caused by formamamidinium iodide (FAI) reaction in the PbI_2 smooth surface, still faces the challenge of producing high quality $FAPbI_3$ films [9].

To overcome these issues, controlling the perovskite crystallization process, escaping defects of films, ensuring a complete surface coverage and reducing grain boundaries are essential [8]. Some strategies for better control and maintenance of the desired crystal phase include the use of ionic additives and hydrohalic acids [10]. Specifically, ammonium thiocyanate (NH_4SCN) is a promising additive candidate due to its effects on perovskites, where $NH_4{}^+$ slows down the crystal growth, reducing defects on the films [11] and SCN^- promotes the formation of the α-phase of $FAPbI_3$, which also improves the stability of the perovskite [12,13].

In this work, we present the combination of the most promising approaches to obtain stable perovskite growth in an open atmosphere: sequential deposition and the use of the pseudohalogen additive ammonium thiocyanate. We studied the introduction of NH_4SCN at different molar concentrations (between 20% and 50%) into the PbI_2 precursor solution in a sequential deposition method. The study will focus on the growth of the films over a glass substrate and then the mechanisms to form the $FAPbI_3$ films, allowing us to understand how the $FAPbI_3$ perovskite grows naturally with the NH_4SCN additive. A unique intermediate layer with different nucleation and growth pathways for $FAPbI_3$ was observed. At 40% concentration, it results in the highest absorption and grain size values, accompanied by a predominance of high crystallinity α-phase, homogeneous morphology, and a slightly lower bandgap than pure $FAPbI_3$. The film with 40% additive concentration exhibits enhanced stability by showing an evident prevalence of α-phase above PbI_2 and δ-phase after 15 days of open atmosphere exposure. The optimized amount of additive is a molar concentration of 40% of NH_4SCN to form $FAPbI_3$ films with optical and structural properties adequate to use in a perovskite solar cell.

2. Materials and Methods

2.1. Materials and Synthesis Process of $FAPbI_3$ Perovskite

All experiments were performed in an open atmosphere following methodologies similar to those reported in [13,14]. Figure 1 exhibits the schematic diagram of the experiment. $FAPbI_3$ films were prepared via the sequential deposition method. In the first step, a precursor solution of 1 M of lead (II) iodide (PbI_2, 99%) and an amount of ammonium thiocyanate (NH_4SCN, ACS reagent, $\geq$97.5%) were mixed in 1 ml of n,n-dimethylformamide (DMF) ($HCON(CH_3)_2$ HPLC $\geq$99.9%) and spin-coated (4000 r.p.m., 60 s) onto a previously cleaned glass substrate and then annealed at 80 °C for 30 min. In the second step, the PbI_2-coated substrate was immersed in a 12 mg/mL solution of formamidinium iodide (CH_5IN_2:FAI) with isopropanol (IPA) at 80 °C for 90 s, followed by an annealed treatment of 170 °C for 60 min to form $FAPbI_3$ films.

The films are identified as 20%, 30%, 40% and 50% according on the amount of NH_4SCN added in the first step.

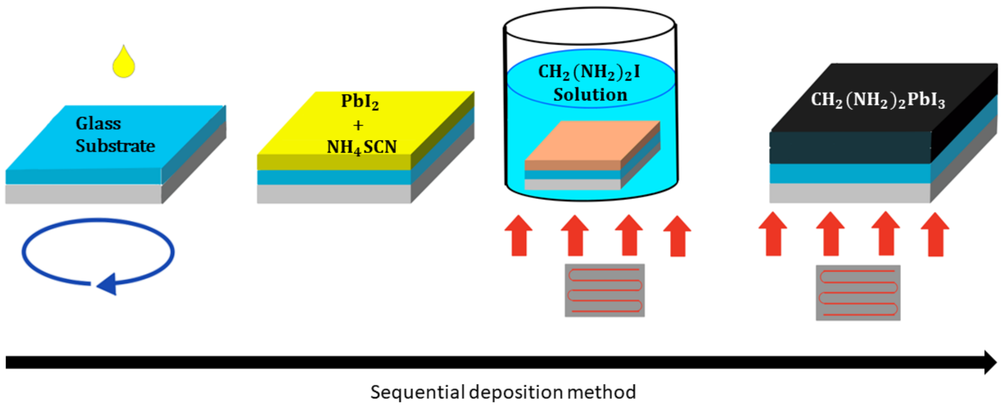

Figure 1. Schematic diagram of perovskite $FAPbI_3$ fabrication by sequential deposition method.

2.2. Characterization

The crystallographic properties of fresh perovskite films were measured by X-ray diffraction equipment (XRD) (D8 Advanced Eco from Bruker, Karlsruhe, Germany) with Cu-Kα radiation of wavelength λ_{Cu} = 1.5418 Å, and scan rate of 6.66 deg/min over the Bragg angle range of 10° to 50°. Degradated perovskite films were measured with XRD equipment (PANALYTICAL EMPYREAN, Malvern Panalytical, Malvern, United Kingdom). The $FAPbI_3$ perovskite crystal size was calculated by taking the value of the full-width at half maximum (FWHM) of the 11.8°, 12.7° and 13.9° peaks. The absorption spectra of the perovskite were recorded by ultraviolet, visible, near-infrared (UV-VIS-NIR) absorption spectroscopy (VARIAN AGILENT CARY 5000, Santa Clara, United States) with a double beam, where the beam reference used was glass substrate. Fresh morphologies of the perovskite films and intermediate layer were characterized on a (Hitachi SU 3500, Tokyo, Japan) scanning electron microscope (SEM) with a low tension of 5.0 kV.

3. Results and Discussion

3.1. $FAPbI_3$ Films

The XRD patterns on glass substrate are shown in Figure 2a. The 20% film exhibits the presence of PbI_2 and $FAPbI_3$ α and δ phases. The peaks at 11.8°, 20.5° and 41.7° belong to δ-$FAPbI_3$, while the peak at 12.7° (001) can be assigned to PbI_2 (JCPDS card no. 79-0803). Peaks at 13.9° (111), 19.8° (012), 24.3° (021), 28.1° (222), 31.5° (123), 40.2° (024), 42.8° (333), and 49.7° are in agreement with α-$FAPbI_3$ [15]. The 30% film also presents $FAPbI_3$ α and δ phases and a reduced signal for PbI_2. Additional peaks at 26°, 31.5° and 32.9° appear for the δ-$FAPbI_3$ phase. For the 40% film, a higher presence of α-phase can be noticed due to the intensity of the 34.5° (030) peak increases. Finally, a mixture of α and δ phases with the predominance of α-phase and the disappearance of the PbI_2 peak is shown in the 50% film.

Furthermore, it can be noted that as the NH_4SCN concentration increases, the following can be observed: a few peaks of δ-$FAPbI_3$ start to decrease gradually until they disappear at 50%. The remaining δ-$FAPbI_3$ continues lowering its intensity. The intensity of the α-$FAPbI_3$ phase peaks at 13.9°, 28.1° and 42.8° increases, while the intensity of peaks at 19.8°, 24.3°, 34.5°, 40.2° and 49.7° decreases.

Figure 2b shows the FWHM of the characteristic peaks of each phase: 11.8°, 12.7° and 13.9° for δ-$FAPbI_3$, PbI_2, and α-$FAPbI_3$, respectively. The estimated crystallite size (c.s.) calculated based on the Scherrer equation ($D=k\lambda/(\beta\cos\theta)$, where D is the crystallite size, k = 0.94, λ_{Cu} = 1.5418 Å, β is the FWHM and θ is the Bragg angle) are imprinted in Figure 2b for each crystalline phase. The 40% film shows the lowest FWHM and the highest estimated crystallite size of 52 nm for α-phase, indicating an improvement of crystallinity [11]. Similar crystallite sizes were reported by Zhu et al. [16].

The absorbance spectra are shown in Figure 3 for films from 20% to 50% of NH_4SCN. The films without NH_4SCN show an absorbance spectrum similar to the one reported by

Mozaffari et al. [14], for films with δ-$FAPbI_3$ phase prevalence which is not beneficial for solar cell applications (Figure S1).

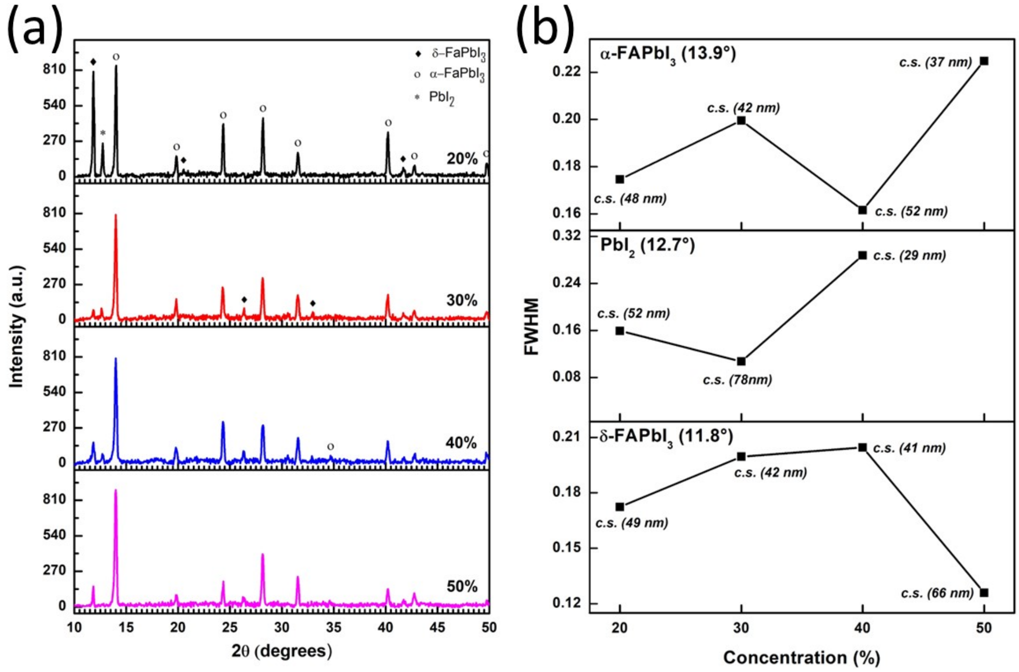

Figure 2. (**a**) XRD patterns and (**b**) FWHM and estimated crystallite size (c.s.) of 11.8°, 12.7°, and 13.9° characteristic peaks of δ-$FAPbI_3$, PbI_2, and α-$FAPbI_3$ phase, respectively, of the perovskite films with different concentration of NH_4SCN.

The absorbance spectra for all the films show the characteristic absorption edge of the α-phase around 800 nm, with a few variations depending on the concentration of NH_4SCN. This is similar to the reported by other authors [10,17]. However, other absorption peaks and behaviors are present from ∼650 nm to ∼300 nm. Therefore, to understand the absorbance spectra, the spectrum of each sample will be discussed in two regions: one over 750 nm and the second from ∼650 nm to ∼300 nm.

It can be seen that the 40% film presents a higher absorption in the visible range associated with the prevalence of α-phase. Imran et al. also observed this; their study showed an improved absorption in the visible range for the photoactive perovskite phase [17]. Furthermore, the 40% film shows a flat profile in the region from 440 nm to 500 nm, indicating the presence of single crystals and a low presence of plumbates (indicated by the red box in Figure 3a). However, the presence of absorption bands in 387, 430, and 509 nm are in agreement with multiplumbate ions of $PbI_3S_3^-$, $PbI_4S_2^{2-}$, PbI_6^{4-}, respectively (marked with an asterisk in Figure 3a) [18], and are consistent with the peak at 12.7°.

As explained, the α-phase presence increases with the NH_4SCN content, accompanied by a decrease or disappearance of the δ-$FAPbI_3$ phase and PbI_2. Consequently, it can be expected that the absorbance spectrum for the α-phase ought to show a significant improvement in the absorption in the visible range. However, films with concentrations other than 40% show a drop of absorbance from ∼800 nm to ∼370 nm. For the 20% and 30% films, this behavior can be attributed to the DMF solvent and the incomplete adhesion of the $FAPbI_3$ film to the glass substrate, as will be shown in SEM micrographs and is in agreement to the previously reported by Kovalenko et al. [18]. The 50% film presents a behavior similar to 20% and 30% films but with better absorption due to the higher presence of α-phase.

The characteristic absorption edge of α-$FAPbI_3$ (Figure 3a) lies in 805, 802, 784, and 800 nm for the 20%, 30%, 40%, and 50% films, respectively. The 20%, 30% and 50% films show a redshift in the absorption edge, from 780 nm to 810 nm. This redshift is related to the increased crystallinity of the α-$FAPbI_3$, as reported by Zhang et al. [19]. Furthermore, these films show a bandgap (E_g) of E_g = 1.40 eV, while the 40% has an E_g value of 1.42 eV, as shown in Figure 3b. These values are slightly lower than the reported for pure α-$FAPbI_3$ (E_g = 1.43 eV) [20]. The decrease in the E_g for 20%, 30%, and 50% films is also associated with the increase in α-$FAPbI_3$ phase crystallinity [21].

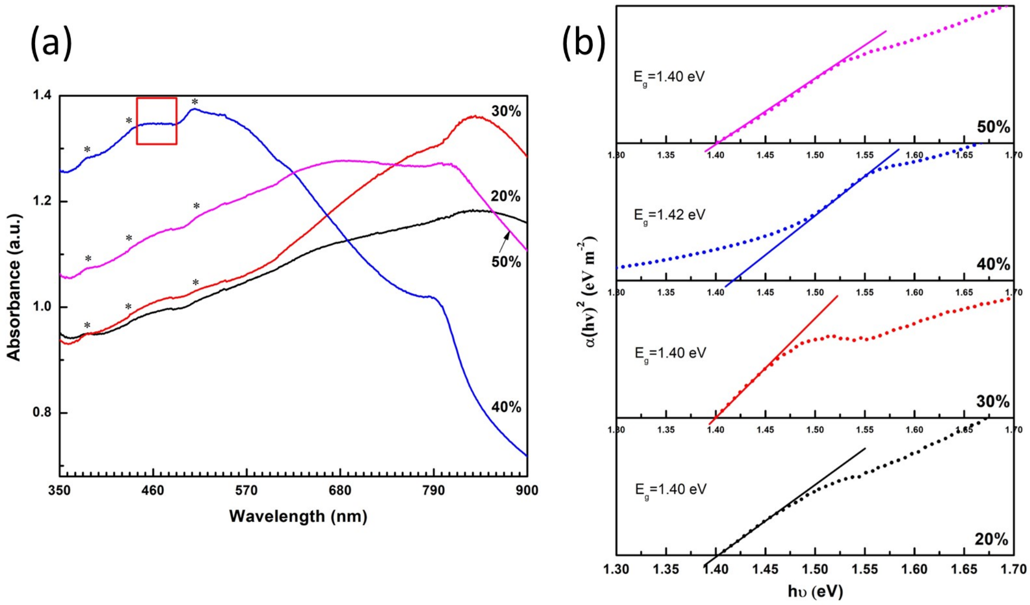

Figure 3. (**a**) Absorbance UV-Vis light spectra indicating the flat profile and the multiplumbate ions of PbI_2 and (**b**) bandgap calculation for the $FAPbI_3$ perovskite films with different concentrations of NH_4SCN.

Figure 4 shows the SEM micrographs of perovskite films. The 20% film is shown in Figure 4a and exhibits an island-like morphology conformed by grains size of ∼950 nm corresponding to the α-$FAPbI_3$ phase [22]. In addition, this can be observed through small precipitates and a large bar-shape of size ∼7 µm (pointed with arrows and a circle, respectively, in Figure 4a) which is in agreement with the EDS, corresponding to PbI_2 (Table S1), confirming the presence of PbI_2 already shown in the XRD of Figure 2a by the 12.7° peak, already reported by Yu et al. [23]. Its noteworthy that what is observed between islands corresponds to the glass substraste, supporting the decrease behavior of the absorbance observed in Figure 3a.

The 30% film is shown in Figure 4b. A non-uniform growth of grains of the size of ∼350 nm and small darker regions corresponding to the glass substrate can be seen. Various studies demonstrated that as NH_4SCN additive increases the grain size, too [24]. However, the mixture of three phases with the predominance of δ-phase reduces grain size [21], and results in the low absorbance behavior discussed earlier. The precipitates associated with the PbI_2 phase changed to a radial finger-shaped (marked with a circle in Figure 4b) of different dimensions, followed by the appearance of PbI_2 points distributed on the film's surface (indicated with arrows in the inset of Figure 4b). The 30% film shows a better adherence which may be associated with an increase in absorbance, relative to 20% film, in the region between 680 and 900 nm.

An improvement in the morphology for 40% film is shown in Figure 4c, as the consequence of homogeneous surface coverage with significantly smaller glass substrate area without film (less than 5%) and larger grains of ∼1350 nm. This change in morphology may be due the higher presence and high crystallinity of α-phase, in addition to the increase in FWHM of δ-phase and intensity reduction of the PbI_2 characteristic peak (Figure 2). Furthermore, the low intensity of the 12.7° peak is in concordance with the size reduction of PbI_2 precipitates. Based on the foregoing, the surface morphology and crystallinity improve the absorbance shown in Figure 3a. Even when the samples show an uneven coverage over glass substrates, it is well known that an appropiate election of the electron transport layer leads to a homogeneous perovskite layer and a reduction of pinholes.

The morphology of the 50% film is shown in Figure 4d. The reduction of surface coverage accompanied by an increment of glass substrate area reduces the absorbance (Figure 3a). It can be observed that the precipitates associated with the PbI_2 phase have no crystalline shape anymore. Consequently, there is no PbI_2 peak in XRD, but the UV-VIS absorption bands confirm the presence of multiplumbates precipitates in the film. However, despite low absorbance, the increased α-phase in 50% film showed a better absorbance regarding 20% and 30%.

It is evident in Figure 4 that adding a proper amount of NH_4SCN to the precursor solution of PbI_2 is related to the formation of an intermediate layer, which leads to a significant change in the morphology of the perovskite films.

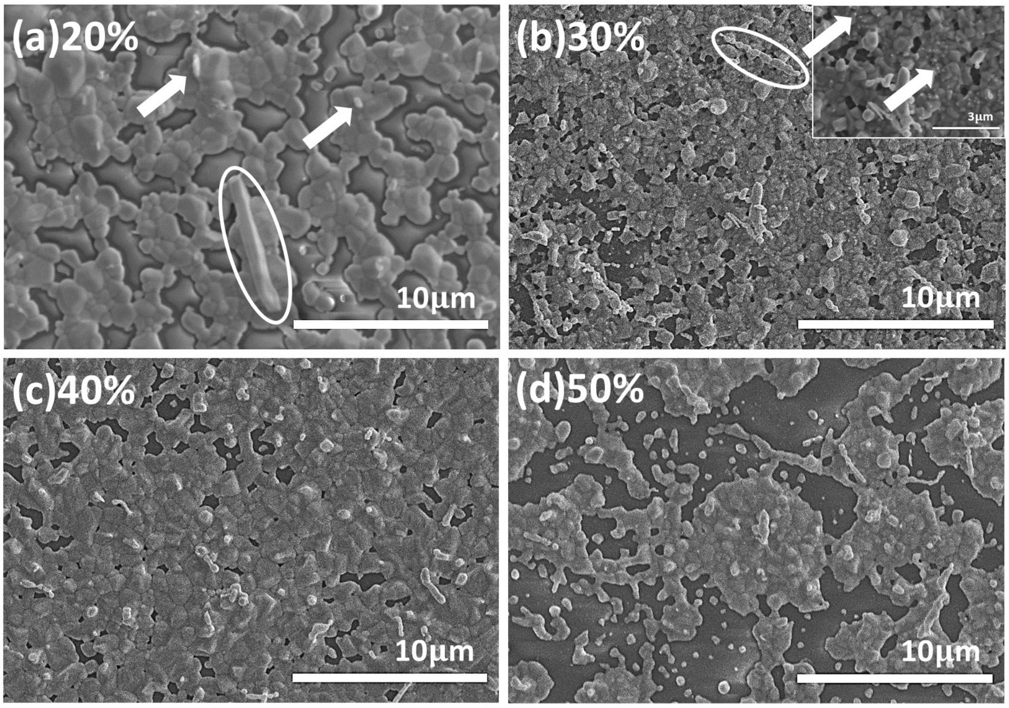

Figure 4. Top-view SEM micrographs of $FAPbI_3$ perovskite films, from (**a**–**d**) 20–50% concentration of NH_4SCN. The small precipitates and the bar-shaped in 20% film are indicated with arrows and a circle, respectively. The radial finger-shaped is marked with a circle in 30% film, and PbI_2 points are highlighted with arrows on the inset of 30% film. The scale bar indicates 10 µm.

3.2. Intermediate Layer

Based on the strong interaction between the atoms due to the similarity of the ionic radius of the cation NH_4^+ with Pb^{2+} and the anion SCN^- (2.15–2.22 Å) with I^- (2.22 Å), respectively [11], it can be inferred that adding NH_4SCN in the precursor solution of PbI_2 would lead to an intermediate layer that may improve the nucleation and growth of the $FAPbI_3$ perovskite. In order to study this phenomenon, XRD patterns of PbI_2 with NH_4SCN films, after being annealed at the first step of the sequential deposition method, were recorded as shown in Figure 5. These films will be named p-20%, p-30%, p-40% and p-50%. An additional percentage of NH_4SCN was included (p-80%) to observe if, at a higher concentration of NH_4SCN, a favorable growth of the final perovskite film is promoted.

P-20% and p-30% films exhibit the characteristic peaks at 12.7° (001), 25.1° (002), and 38.6° (003) of PbI_2. From p-40% onwards, an ionic substitution of the I^- to the SCN^- anions are promoted. This can be observed with the rise of the diffraction peak intensity at

21.5°, corresponding to $Pb(SCN)_2$. This ionic substitution was to be expected based on the chemical similarity of the pseudohalogen (SCN) with the halogen (I) [25].

As the NH_4SCN concentration increases, the intensity of the peaks corresponding to the PbI_2 phase shows a reduction, the estimated crystallite size increases from 42 nm for p-20% to 44 nm for p-50% while the $Pb(SCN)_2$ peak becomes more intense than the p-20%. Finally, it is interesting that for p-80%, additional peaks appear at 25.5° (011) and 34.3° (102), corresponding to PbI_2 and another one at 44.1° (110) which is associated with NH_4SCN [26]. This suggests that NH_4SCN, at higher concentrations, neither evaporates completely, nor fully reacts with PbI_2, resulting in remanents on the film. (More information of 80% films can be found in Supplementary Material.)

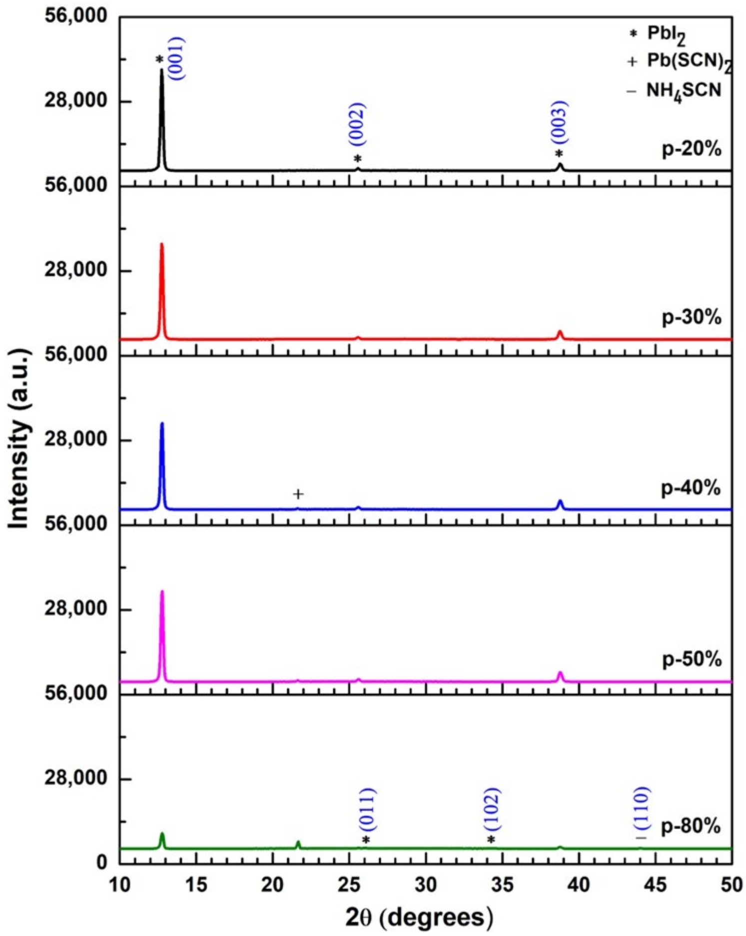

Figure 5. XRD patterns of intermediate layer from p-20% to p-80% concentration of NH_4SCN.

Despite the intensity increment of the $Pb(SCN)_2$ peaks observed in the intermediate layer, in the $FAPbI_3$ XRD patterns, illustrated in Figure 3a, there is no trace of $Pb(SCN)_2$. It has been previously reported that at the first annealing process part of NH_4SCN evaporates by separating in NH_3 and HSCN due to the low stability of the NH_4SCN molecule [27], leaving only a trace of S, C, and N distributed in the surface. This phenomenon was also observed by Lin and Cai et al. [24,28] and corroborated in this work by EDS (Table S2). At the EDS analysis in the $FAPbI_3$ film, the S signal was weaker than the signal showed in the PbI_2 intermediate layer, confirming that most of the S could evaporate during the second annealing process (Table S3). This reveals the importance of NH_4SCN in the change in morphology.

Figure 6a–d presents the SEM micrographs of the intermediate layer according to NH_4SCN concentration. The P-20% film exhibits irregular porous morphology with nearly complete coverage. Needle-like precipitates are barely present on the surface, and the film seems composed of multilayers. The p-30% film is more homogeneous with a smoother surface and better coverage than p-20%. Some holes with an elongate shape can be observed. The intensity reduction of PbI_2 peaks with the increasing $Pb(SCN)_2$ peaks discussed earlier gives rise to more significant morphological changes from p-30% to p-40% and above films.

The p-40% film shows a flake morphology, interconnected by porous branches that seem in upper and lower layers with higher substrate area. At p-50%, the wafer-shapes are entirely defined, surrounded by crystalline aligned precipitates that generate a star-shape morphology. A fibrous and porous morphology is also present in the film, covering the remaining area of the glass substrate.

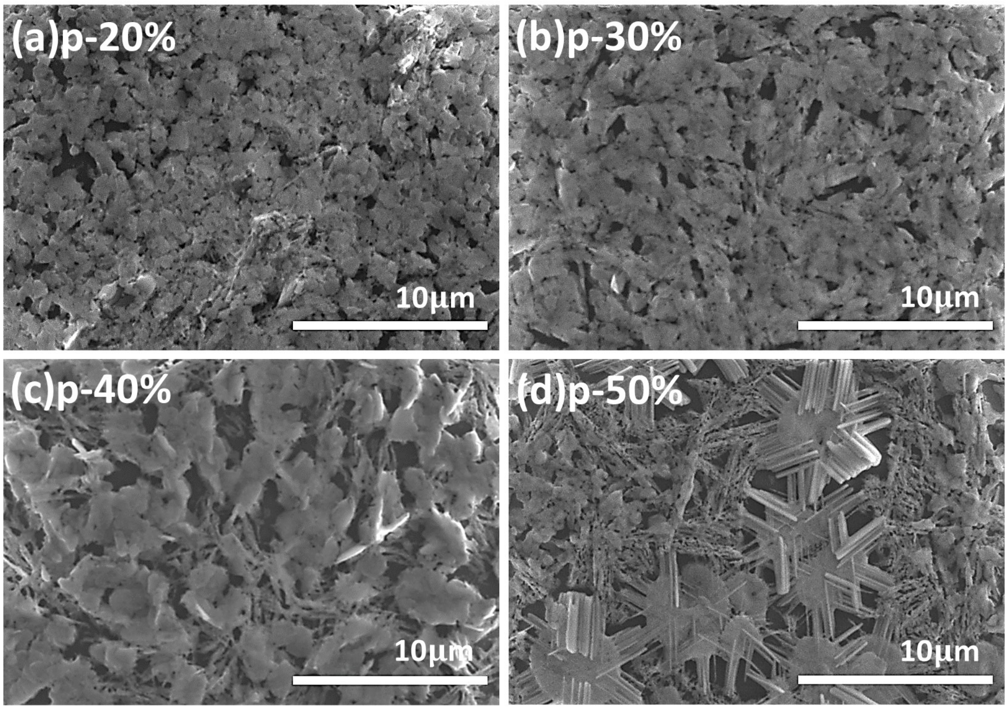

Figure 6. Top-view SEM micrographs of intermediate layers from (**a**–**d**) p-20% to p-50% concentration of NH_4SCN. The scale bar indicates 10 μm.

Ke et al. reported that with only 5% of $Pb(SCN)_2$ added to the perovskite precursor, grains can reach sizes of 2 μm [29]. In this study, the concentration of NH_4SCN provokes significant morphological changes and raises the intensity of $Pb(SCN)_2$ peak at the intermediate layer but not in the final perovskite film. the morphology changed from irregular porous to fiber-like as a higher amount of NH_4SCN and $Pb(SCN)_2$ was added.

For the precipitates described in p-50% film, the additive increment causes an increment of S and a decline of I (Table S4). It can be assumed that the major presence of sulfur generates multiplumbate ions that correspond to the precipitates. The PbI_2 atomic weight seems to correspond to the irregular morphology of p-20% and p-30%, flakes of p-40%, and wafers of p-50% (Table S5).

The temporary ionic substitution at the first step makes SCN ion highly suitable for forming hydrogen bonds with $CH(NH_2)_2$ [30]. Furthermore, the higher enthalpy and electronegativity of SCN than iodine [31] promotes the reaction of the SCN with FAI solution at the second step of deposition. Accompanied by a constant reduction of PbI_2 peaks in the intermediate layer, avoiding secondary phases and encouraging a quick conversion for the $FAPbI_3$ film [32].

The intermediate layer acts as a nucleation structure for the $FAPbI_3$ perovskite, in which it forms and grows through the architecture of each additive concentration. The morphology, the crystallinity and the phases in perovskite $FAPbI_3$, depend on the immersion time, r.p.m. of the spin coating at first step, and the quantity of NH_4SCN.

Dong et al. found that by increasing the immersion time, a gradual grain size elongation can be seen in the $FAPbI_3$ film [27]. In this work, it can be observed that the concentration of NH_4SCN generates an increment in grain size. Moreover, the higher immersion time results in an excessive elongation of the film. If to the foregoing high-r.p.m. spin coating is added at the first step, a low cover of the substrate area is to be expected. This phenomenon was also observed by Tai et al., concluding that with higher than 4000 r.p.m., a full coverage of the surface will not be obtained [12].

In the same way, immersion with a surplus of time could extract an excess of organic cation $CH(NH_2)_2{}^+$, causing its dissolution in the IPA solution and leading to incomplete conversion of PbI_2 to perovskite [33]. This may explain the presence of the δ-phase even with the high concentrations of NH_4SCN that promote the α-phase.

It can be observed that the seeming multilayers, the porous in the irregular morphology, and the flakes morphology as well as in the branches of the p-20% and p-40% films, respectively, promote the nucleation and growth of $FAPbI_3$ perovskite film by allowing the diffusion of FAI solution in a larger quantity of vacant spaces. This results in the nucleation and growth of a more homogeneous $FAPbI_3$ perovskite film with larger grain size. Similarly, Moreno et al. [34] observed that a porous layer of PbI_2 promotes the diffusion of methylammonium iodide (MAI) solution into the film, leading to a better reaction with PbI_2.

Apart from that, p-30% film has a smooth morphology on most of its surface, and p-50% has wafers with smooth surfaces. These intermediate smooth morphologies will not allow the diffusion of FAI solution, enabling only to react with the PbI_2 on the surface, resulting in a non-uniform growth and the prevalence of PbI_2 and δ-phase due to an incomplete conversion to $FAPbI_3$. Fu et al. also observed this phenomenon, proving the initial formation of $MAPbI_3$ on the surface, obstructing the diffusion of MAI for a complete reaction with PbI_2 [35]. The fiber-like morphology of the p-50% film is too thin, resulting in a dilution of the fiber-like intermediate architecture during the immersion in FAI, leaving a poor intermediate layer for perovskite nucleation.

It must be noted that the 40% film has the biggest grain size and more homogeneous film compared to the rest . This may be due to a preferential balance between the DMF, NH_4SCN and PbI_2 enhancing the ionic substitution of SCN^- in the intermediate layer accompanied by and optimum immersion time that, in addition, promotes the α-phase. The prior properties enhance not only a good quality film, but a more stable perovskite film.

3.3. Stability of Perovskite Films

In order to explore the perovskite films stability, perovskites were aged for 15 days prior to XRD measurements. The XRD patterns (Figure S2) show that all peaks have a slight displacement to higher angles due to a distortion in the crystalline lattice [36]. There is also an increase in δ-phase at the expense of a reduction in α-phase. This, along with the appearance of peaks associated with PbI_2, $Pb(SCN)_2$ and FAI are related to the films' degradation.

The highest prevalence of α-phase in 20% and 40% films are attributed to the morphology of both films with less grain boundaries and homogeneity, which enhanced the stability against moisture and increased the lifetime of the films. Otherwise, the higher intensity of PbI_2 and δ-phase in the 30% and 50% films are in agreement with the morphology with more grain boundaries and with small grain size, which allows the infiltration of moisture, as was observed by another author [37].

Finally, it is known that mixed α/δ-phases make the films thermodynamically stable due to the mixing of both entropies [38], which in agreement with the results of this work, the presence of mixed α/δ-phase in the fresh perovskite and degradated perovskite films, result in a favorable change in the entropy to reduce phase conversion. The films in this work present a higher stability compared with recent work where a complete degradation of δ-phase to α-phase was reported [39].

4. Conclusions

In this work, an experimental method to obtain $FAPbI_3$ over a glass substrate in a sequential deposition method in an open atmosphere was reported. The impact of an intermediate layer fabricated with additive NH_4SCN introduced in the precursor solution of PbI_2 was studied. The intermediate layer acts as a nucleation structure for the $FAPbI_3$ in which it forms and grows through the architecture of each additive concentration. In 40% of NH_4SCN concentration film, the perovskite shows a slightly lower bandgap than pristine $FAPbI_3$, predominance of α-phase with enhanced crystallinity, more significant absorption in visible range and homogenous granular coverage with a grain size of ∼1350 nm. It appears that the multilayers and the porous structure in the irregular morphology in p-40% allowed the perovskite film to grow favorably. Consequently, the 40% film shows enhanced stability due the morphology and the entropy change by the mixed α/δ-phase. The presence of SCN in the films is fundamental to raising the decomposition energy of the $FAPbI_3$, and the open atmosphere enhanced the stability against atmosphere factors. It can be concluded that adding an adequate concentration of NH_4SCN in the precursor solution of a sequential deposition method leads to a favorable path for growing $FAPbI_3$ for use in solar cells.

Supplementary Materials: The following supporting information can be downloaded at: https://www.mdpi.com/article/10.3390/cryst13050795/s1, Table S1. Elemental analysis by energy-dispersive X-ray on bar-shaped morphology in 20% film; Table S2. Elemental Analysis by energy-dispersive X-ray of p-40% film after first annealing; Table S3. Elemental Analysis by energy-dispersive X-ray of 40% film after second annealing; Table S4. Elemental Analysis by energy-dispersive X-ray of p-50% film over a precipitate; Table S5. Elemental Analysis by energy-dispersive X-ray of p-50% film over a waffle morphology; Figure S1. Absorbance spectrum of pristine $FAPbI_3$ (0% of NH_4SCN); Figure S2. Comparative XRD patterns between fresh $FAPbI_3$ and degradated $FAPbI_3$ with different concentration of NH_4SCN; Figure S3. Top-view SEM micrograph of p-80% film. The white scale bar indicates 10 µm. Figure S4. Top-view SEM micrograph of $FAPbI_3$ perovskite film with 80% concentration of NH_4SCN. White scale bar indicates 10 µm; Figure S5. Absorbance UV-Vis light spectra of $FAPbI_3$ perovskite films with different concentration of NH_4SCN including 80%; Figure S6. XRD patterns of the $FAPbI_3$ perovskite film with 80% concentration of NH_4SCN.

Author Contributions: Conceptualization, J.L.M.-Z., M.C.E.-E. and C.J.D.-G.; methodology, J.L.M.-Z., M.C.E.-E., F.C.-S. and C.J.D.-G.; validation, J.L.M.-Z., M.C.E.-E. and C.J.D.-G.; formal analysis, J.L.M.-Z. and C.J.D.-G.; investigation, J.L.M.-Z., M.C.E.-E., F.C.-S. and C.J.D.-G.; resources, M.C.E.-E., F.C.-S. and C.J.D.-G.; data curation, J.L.M.-Z., M.C.E.-E., F.C.-S. and C.J.D.-G.; writing—original draft preparation, J.L.M.-Z. and C.J.D.-G.; writing—review and editing, J.L.M.-Z., M.C.E.-E., F.C.-S. and C.J.D.-G.; supervision, M.C.E.-E. and C.J.D.-G.; project administration, J.L.M.-Z., M.C.E.-E. and C.J.D.-G. All authors have read and agreed to the published version of the manuscript.

Funding: This research received scholarship from the Mexican government institution CONACyT for the doctoral studies of J.L.M.-Z.; F.C.-S. acknowledges funding from CONACYT Synergy project 1564464; F.C.-S. also received funding from FICSAC and FISMAT at Universidad Iberoamericana Ciudad de Mexico; C.J.D.-G. acknowledges funding from VIEP-BUAP 2023.

Data Availability Statement: The data presented in this study are available on request from the corresponding author.

Acknowledgments: The authors give thanks to Ulises Salazar Kuri for his help in the measurement of degradated XRD perovskite films. José Adrián Díaz Hernández, Josué Hernández and Alma Cuellar for his support and knowledge to conduct all the experiments. Jorge Luis Miró Zárate thanks to Mexican government institution CONACyt and Instituto Tecnológico y de Estudios Superiores de Monterrey for its support through a doctoral studies scholarship.

Conflicts of Interest: The authors declare no conflict of interest.

Abbreviations

The following abbreviations are used in this manuscript:

NH_4SCN	Ammonium Thiocyanate
PBI_2	Lead (II) Iodide
$FAPbI_3$	Formamidinium Lead Halide
I	Iodine
SCN	Thiocyanate
HOIP	Hybrid Organic-Inorganic Perovskite
PCE	Power Conversion Efficiency
$MAPbI_3$	Methylammonium Lead Halide
FAI	Formamidinium Iodide
NH_4	Ammonium
DMF	Dimethylformamide
r.p.m.	Revolution Per Minute
IPA	Isopropanol
UV-VIS-NIR	Ultraviolet Visible Near Infrared
SEM	Scanning Electron Microscope
XRD	X Ray Difraction
FWHM	Full Width at Half Maximum
E_g	Bandgap
$Pb(SCN)_2$	Lead (II) Thiocyanate
EDS	Energy Dispersive Espectroscopy
MAI	Methylammonium Iodide

References

1. Brenner, T.M.; Egger, D.A.; Kronik, L.; Hodes, G.; Cahen, D. Hybrid organic-inorganic perovskites: low-cost semiconductors with intriguing charge-transport properties. *Nat. Rev. Mater.* **2016**, *1*, 15007. [CrossRef]
2. Wang, R.; Mujahid, M.; Duan, Y.; Wang, Z.K.; Xue, J.; Yang, Y. A Review of Perovskites Solar Cell Stability. *Adv. Funct. Mater.* **2019**, *29*, 1808843. [CrossRef]
3. Ava, T.T.; Al Mamun, A.; Marsillac, S.; Namkoong, G. A Review: Thermal Stability of Methylammonium Lead Halide Based Perovskite Solar Cells. *Appl. Sci.* **2019**, *9*, 188. [CrossRef]
4. Chen, Q.; Marco, N.D.; Song, T.B. Under the spotlight: The organic-inorganic hybrid halide perovskite for optoelectronic applications. *Nano. Today* **2015**, *10*, 355. [CrossRef]
5. Conings, B.; Drijkoningen, J.; Gauquelin, N.; Babayigit, A.; D'Haen, J.; D'Olieslaeger, L.; Ethirajan, A.; Verbeeck, J.; Manca, J.; Mosconi, E.; et al. Intrinsic Thermal Instability of Methylammonium Lead Trihalide Perovskite. *Adv. Energy Mater.* **2015**, *5*, 1500477. [CrossRef]
6. Li, Y.; Zhang, T.; Xu, F.; Wang, Y.; Li, G.; Yang, Y.; Zhao, Y. CH_3NH_3Cl Assisted Solvent Engineering for Highly Crystallized and Large Grain Size Mixed-Composition $(FAPbI_3)_{0.85}(MAPbBr_3)_{0.15}$ Perovskites. *Crystals* **2017**, *7*, 272. [CrossRef]
7. Ummadisingu, A.; Grätzel, M. Revealing the detailed path of sequential deposition for metal halide perovskite formation. *Sci. Adv.* **2018**, *4*, e1701402. [CrossRef]
8. Chen, H.; Chen, Y.; Zhang, T.; Liu, X.; Wang, X.; Zhao, Y. Advances to High-Performance Black-Phase $FaPbI_3$ Perovskite for efficient and stable Photovoltaics. *Small Struct.* **2021**, *2*, 2000130–2000145. [CrossRef]
9. Wang, J.F.; Zhu, L.; Zhao, B.G.; Zhao, Y.L.; Song, J.; Gu, X.Q.; Qiang, Y.H. Surface engineering of perovskite films for efficient solar cells. *Sci. Rep.* **2017**, *7*, 14478. [CrossRef]
10. Lyu, M.; Park, N.G. Effect of Additives FA, MA, Cs, Rb, NH_4, Cl, Br, I) in $FAPbI_3$ on Photovoltaic Parameters of Perovskite Solar Cells. *Solar RRL* **2020**, *4*, 20000331. [CrossRef]
11. Zhang, H.; Hou, M.; Xia, Y.; Wei, Q.; Wang, Z.; Cheng, Y.; Chen, Y.; Huang, W. Synergistic effect of anions and cations in additives for highly efficient and stable perovskite solar cells. *J. Mater. Chem.* **2018**, *6*, 9264–9270. [CrossRef]
12. Tai, Q.; You, P.; Sang, H.; Liu, Z.; Hu, C.; Chan, H.L.; Yan, F. Efficient and stable perovskite solar cells prepared in ambient aire irrespective of the humidity. *Nat. Commun.* **2016**, *7*, 11105. [CrossRef]
13. Lu, H.; Liu, Y.; Ahlawat, P.; Mishra, A.; Tress, W.R.; Eickemeyer, F.T.; Yang, Y.; Fu, F.; Wang, Z.; Avalos, C.E.; et al. Vapor-assisted deposition of highly efficient, stable black-phase $FAPbI_3$ perovskite solar cells. *Science* **2020**, *370*, eabb8985. [CrossRef]
14. Mozaffari, M.; Behjat, A.; Mirjalili, B.F. The effect of solution process control on the formation of the α-$FAPbI_3$ perovskite: $FAPbI_3$ versus $MAPbI_3$ solar cells. *Sol. Energy* **2018**, *174*, 780–785. [CrossRef]
15. Yang, S.; Liu, W.; Zuo, L.; Zhang, X.; Chen, J.; Li, C.Z.; Wu, G.; Chen, H. Thiocyanate Assisted Performance Enhancement for Formamidinium Based Planar Perovskite Solar Cells through Single One-step Solution Process. *J. Mater. Chem.* **2016**, *4*, 9430–9436. [CrossRef]
16. Zhu, L.; Cao, H.; Xue, C.; Zhang, H.; Qin, M.; Wang, J.; Wen, K.; Fu, Z.; Jiang, T.; Xu, L.; et al. Unveiling he additivie-assisted oriented growth of perovskite crystallite for high performance light-emitting diodes. *Nat. Commun.* **2021**, *12*, 5081. [CrossRef]
17. Imran, M.; Khan, N. Perovskite phase formation in formamidinium–methylammonium lead iodide bromide $(FAPbI_3)_{1-x}(MAPbBr_3)_x$ materials and their morphological, optical and photovoltaic properties. *Appl. Phys.* **2019**, *125*, 575. . [CrossRef]

18. Rahimnejad, S.; Kovalenko, A.; Forés, S.M.; Aranda, C.; Guerrero, A. Coordination Chemistry Dictates the Structural Defects in Lead Halide Perovskites. *ChemPhysChem* **2016**, *17*, 2795–2798. [CrossRef]
19. Zhang, Y.; Seulgi, K.; Lee, D.K.; Park, N. $CH_3NH_3PbI_3$ and $HC(NH_2)_2PbI_3$ Powders Synthesized from Low-Grade PbI_2: Single Precursor for High-Efficiency Perovskite Solar Cells. *ChemSusChem* **2018**, *11*, 1813–1823. [CrossRef]
20. Targhi, F.F.; Jalili, Y.S.; Kanjouri, F. $MAPbI_3$ and $FAPbI_3$ perovskites as solar cells: Case study on structural, electrical and optical properties. *Results Phys.* **2018**, *10*, 616–627. [CrossRef]
21. Ma, F.; Li, J.; Li, W.; Lin, N.; Wang, L.; Qiao, J. Stable α/δ phase junction of formamidinium lead iodide perovskites for enhuanced near-infrared emission. *Chem. Sci.* **2017**, *8*, 800–805. [CrossRef] [PubMed]
22. Yang, F.; Dong, L.; Jang, D.; Tam, K.C.; Zhang, K.; Li, N.; Guo, F.; Li, C.; Arrivé, C.; Bertrand, M.; et al. Fully Solution Processed Pure α-Phase Formamidinium Lead Iodide Perovskite Solar Cells for Scalable Production in Ambient Condition. *Adv. Energy Mater.* **2020**, *10*, 2001869. [CrossRef]
23. Yu, Y.; Wang, C.; Grice, C.R.; Shrestha, N.; Chen, J.; Zhao, D.; Liao, W.; Cimaroli, A.J.; Roland, P.J.; Ellingson, R.J.; et al. Improving the Performance of Formamidinium and Cesium Lead Triiodide Perovskite Solar Cells using Lead Thiocyanate Additives. *ChemSusChem* **2016**, *9*, 3288–3297. [CrossRef] [PubMed]
24. Lin, P.Y.; Loganathan, A.; Raifuku, I.; Li, M.H.; Chiu, Y.Y.; Chang, S.T.; Fakharuddin, A.; Lin, C.F.; Guo, T.F.; Schmidt-Mende, L.; et al. Pseudo-Halide Perovskite Solar Cells. *Adv. Energy Mater.* **2021**, *11*, 2100818. [CrossRef]
25. Balaji, G.; Joshi, P.H.; Abbas, H.A.; Zhang, L.; Kottokkaran, R.; Samiee, M.; Noack, M.; Dalal, V.L. $CH_3NH_3PbI_3$ from non-iodide lead salts for perovskite solar cells via the formation of PbI_2. *Phys. Chem. Chem. Phys.* **2015**, *17*, 10369–10372. [CrossRef]
26. Zhang, J.; Song, Y.; Dong, X.; Jiang, H.; Tang, J.; Li, H. Umbrella-like CdS single crystal: exposed (002) facets and enhanced photocatalytic properties. *J. Mater. Sci.* **2020**, *55*, 11167–11176. [CrossRef]
27. Dong, H.; Wu, Z.; Xi, J.; Xu, X.; Zuo, L.; Lei, T.; Zhao, X.; Zhang, L.; Hou, X.; Jen, A.K.Y. Pseudohalide-Induced Recrystallization Engineering for $CH_3NH_3PbI_3$ Film and Its Application in Highly Efficient Inverted Planar Heterojunction Perovskite Solar Cells. *Adv. Funct. Mater.* **2018**, *28*, 1704836. [CrossRef]
28. Cai, Y.; Wang, S.; Sun, M.; Li, X.; Xiao, Y. Mixed cations and mixed halide perovskite solar cell with lead thiocyanate additive for high efficiency and long-term moisture stability. *Org. Electron.* **2018**, *53*, 249–255. [CrossRef]
29. Ke, W.; Xiao, C.; Wang, C.; Saparov, B.; Duan, H.S.; Zhao, D.; Xiao, Z.; Schulz, P.; Harvey, S.P.; Liao, W.; et al. Employing Lead Thiocyanate Additive to Reduce the Hysteresis and Boost the Fill Factor of Planar Perovskite Solar Cells. *Adv. Mater.* **2016**, *28*, 5214–5221. [CrossRef]
30. Lou, Y.; Niu, Y.; Yang, D.; Xu, Q.; Hu, Y.; Shen, Y.; Ming, J.; Chen, J.; Zhang, L.; Zhao, Y. Rod-shaped thiocyanate-induced abnormal band gap broadening in SCN^- doped $CsPbBr_3$ perovskite nanocrystals. *Nano Res.* **2018**, *11*, 2715–2723. [CrossRef]
31. Ahrl, S.T.; Björk, N.O.; Portanova, R.O. Metal halide and pseudohalide complexes in Dimethyl sulfoxide solution. VI. Enthalpy measurements on the Zinc(II) Chloride, Bromide, Iodide and Thiocyanate Systems. *Acta Chem. Scand.* **1976**, *30a*, 270–276. [CrossRef]
32. Chen, Y.; Li, B.; Huang, W.; Gao, D.; Liang, Z. Efficient and reproducible $CH_3NH_3PbI_{(3-x)}(SCN)_x$ perovskite based planar solar cells. *Chem. Commun.* **2015**, *60*, 11997–9. [CrossRef]
33. Park, B.W.; Kwon, H.W.; Lee, Y.; Lee, D.Y.; Kim, M.G.; Kim, G.; Kim, K.j.; Kim, Y.K.; Im, J.; Shin, T.J.; et al. Stabilization of formamidinium lead triiodide alpha-phase with isopropylammonium chloride for perovskite solar cells. *Nat. Energy* **2021**, *6*, 419–428. [CrossRef]
34. Moreno-Romero, P.M.; Rodríguez-Castañeda, C.A.; Corpus-Mendoza, A.N.; Torres-Herrera, D.M.; Prias-Barragán, J.J.; Hu, H. Formation of a nanoporous PbI_2 layer framework via 4-tBP additive to improve the performance and stability of two-step prepared hybrid perovskite solar cells under ambient conditions. *Int. J. Energy Res.* **2022**, *46*, 23133–23144. [CrossRef]
35. Fu, Y.; Meng, F.; Rowley, M.B.; Thompson, B.J.; Shearer, M.J.; Ma, D.; Hamers, R.J.; Wright, J.C.; Jin, S. Solution Growth of Single Crystal Methylammonium Lead Halide Perovskite Nanostructures for Optoelectronic and Photovoltaic Applications. *J. Am. Chem. Soc.* **2015**, *137*, 5810–5818. [CrossRef]
36. Jin, B.; Cao, J.; Yuan, R.; Cai, B.; Wu, C.; Zheng, X. Strain Relaxation for Perovskite Lattice Reconfiguration. *Adv. Energy Sustain. Res.* **2022**, *4*, 2200143. [CrossRef]
37. D'Innocenzo, V.; Srimath Kandada, A.R.; De Bastiani, M.; Gandini, M.; Petrozza, A. Tuning the Light Emission Properties by Band Gap Engineering in Hybrid Lead Halide Perovskite. *J. Am. Chem. Soc.* **2014**, *136*, 17730–17733. [CrossRef]
38. Yi, C.; Luo, J.; Meloni, S.; Boziki, A.; Ashari-Astani, N.; Grätzel, C.; Zakeeruddin, S.M.; Röthlisberger, U.; Grätzel, M. Entropic stabilization of mixed A-cation ABX_3 metal halide perovskites for high performance perovskite solar cells. *Energy Environ. Sci.* **2016**, *9*, 656–662. [CrossRef]
39. Raval, P.; Kennard, R.M.; Vasileiadou, E.S.; Dahlman, C.J.; Spanopoulos, I.; Chabinyc, M.L.; Kanatzidis, M.; Manjunatha Reddy, G.N. Understanding Instability in Formamidinium Lead Halide Perovskites: Kinetics of Transformative Reactions at Grain and Subgrain Boundaries. *ACS Energy Lett.* **2022**, *7*, 1534–1543. [CrossRef]